

NEUROSYSTEMS

Local field potentials are local events in the mouse auditory cortex

Xiuping Liu, Linran Zhou, Fangchao Ding, Yehan Wang and Jun Yan

Department of Physiology and Pharmacology, Hotchkiss Brain Institute, Cumming School of Medicine, University of Calgary, 3330 Hospital Drive NW, Calgary, AB, T2N 4N1, Canada

Keywords: auditory cortex, local field potential, mouse, neuronal receptive field, spike, systems neuroscience

Abstract

Local field potentials (LFPs) and spikes (SPKs) sampled at the thalamocortical recipient layers represent the inputs from the thalamus and outputs to other layers. Previous studies have shown that SPK-constructed receptive fields (RF_{SPK}) of cortical neurons are much smaller than LFP-constructed RFs (RF_{LFP}). The difference in cortical RF_{LFP} and RF_{SPK} is therefore a plausible indication of local networking. The presence of a boarder RF_{LFP} appears due to contamination, to some degree, from remote sites. Our studies of the mouse primary auditory cortex show that the best frequencies and minimum thresholds of RF_{SPK} and RF_{LFP} were similar. We also observed that the RF_{LFP} area was only slightly larger than the RF_{SPK} area, a very different finding from previous reports. The bandwidth of RF_{LFP} was slightly broader than that of RF_{SPK} at all levels. These data do not support the explanation that bioelectrical signals from distant sites impact on cortical LFP through volume conduction. That the cortical LFP represents a local event is further supported by comparisons of RF_{SPK} and RF_{LFP} after cortical inhibition by muscimol and cortical disinhibition by bicuculine. We conclude that the difference between RF_{SPK} (output of cortical neurons) and RF_{LFP} (input of cortical neurons) results from intracortical processing, including cortical lateral inhibition and excitation.

Introduction

Neurons in deep layer III and layer IV of the primary sensory cortex are primarily driven by thalamocortical inputs (Kyriazi & Simons, 1993; Miller *et al.*, 2001; Hirsch, 2003; Metherate *et al.*, 2005; Barkat *et al.*, 2011; Hackett *et al.*, 2011). The output of cortical neurons is not simply the summation of thalamocortical inputs; it is shaped by the networking of cortical local circuitry (Eggermont, 1996; Noreña & Eggermont, 2002; Kenet *et al.*, 2003; Fiser *et al.*, 2004; Kaur *et al.*, 2004; Metherate *et al.*, 2004; Kurt *et al.*, 2007; Berens *et al.*, 2008; Rasch *et al.*, 2009; Liu & Galindo-Leon, 2010; Happel *et al.*, 2010; Moeller *et al.*, 2010; Eggermont *et al.*, 2011). Acquiring new insights into the workings of local cortical networks continues to challenge neuroscientists.

Auditory information processing at the recipient layers of the sensory cortex has been studied by comparing cortical local field potentials (LFPs) that represent the inputs of cortical neurons and the spike activities (SPKs) that represent the outputs of cortical neurons (Lorente de No, 1947; Eccles, 1951; Eggermont, 1996; Chrobak & Buzsáki, 1998; Buzsáki & Draguhn, 2004; Metherate *et al.*, 2004; Lakatos *et al.*, 2005; Mormann *et al.*, 2005; Canolty *et al.*, 2006; Einevoll *et al.*, 2007; Katzner *et al.*, 2009; Kelly *et al.*, 2010; Denker *et al.*, 2010, 2011; Eggermont *et al.*, 2011). In animals such as monkeys and cats, the LFP-constructed receptive field (RF_{LFP}) and the SPK-constructed receptive field (RF_{SPK}) of auditory cortical neurons are mostly

similar in their best frequencies (BFs) but show large differences in their spectral ranges. The bandwidth of RF_{LFP} can be much greater than that of RF_{SPK} , particularly at high sound levels (Eggermont, 1996, 1998; Noreña & Eggermont, 2002; Kaur *et al.*, 2004; Machens *et al.*, 2004; Metherate *et al.*, 2004; Noreña *et al.*, 2008; Kajikawa & Schroeder, 2011; Gaucher *et al.*, 2012). The sharper RF_{SPK} , i.e. the outputs of cortical neurons, signifies the manipulation or processing of auditory information in cortical circuitry. Although cortical processing is complex, cortical inhibition mediated by γ -aminobutyric acid receptor A ($GABA_{AR}$) is believed to significantly influence the outputs of cortical neurons (Muller & Scheich, 1988; Hirsch *et al.*, 1998; Wang *et al.*, 2000, 2002; Foeller *et al.*, 2001; Noreña & Eggermont, 2002; Wehr & Zador, 2005; Eggermont *et al.*, 2011; de Cheveigné *et al.*, 2013). A long-standing and critical issue is whether the broader RF_{LFP} can be partly attributed to signals from remote sites due to volume conduction (Kajikawa & Schroeder, 2011).

We addressed this issue by examining the RF_{LFP} and RF_{SPK} of the mouse primary auditory cortex. We found that the RF_{LFP} was only slightly broader than RF_{SPK} and both RF_{SPK} and RF_{LFP} were only slightly broadened by microiontophoresis of the $GABA_{AR}$ antagonist bicuculine. Using paired recordings with $\sim 100 \mu\text{m}$ separation, we discovered that microiontophoresis of the $GABA_{AR}$ agonist muscimol resulted in the complete elimination of activity in one site but not the other.

Materials and methods

Thirty-seven female C57 mice 4–5 weeks old and weighing 15.5–21 g were used in our study. All procedures were in accordance

Correspondence: Dr J. Yan, as above.
E-mail: juyan@ucalgary.ca

Received 10 February 2015, revised 5 June 2015, accepted 18 June 2015

with the Canadian Council on Animal Care and approved by the Health Science Animal Care Committee at the University of Calgary (Protocol number M10029).

Animal preparation

All experiments were performed under anesthesia. Before surgery, the mouse was anesthetized using an intraperitoneal (i.p.) injection of ketamine and xylazine; the initial dose was 85 and 15 mg/kg, respectively. The anesthetic level was examined about every 40 min by stimulation of the mouse tail. If the mouse showed any response to tail stimulation, an additional dose of ketamine (17 mg/kg, i.p.) and xylazine (3 mg/kg, i.p.) was administered. The mouse was mounted on a custom-made head holder that was placed in a sound-proof chamber. The mouse head was immobilized by clamping the palate and nasal bone. After clipping the scalp hair with scissors, the skull was exposed by making a midline incision and removing the connective tissue and muscle. The position of the mouse head was adjusted to align the bregma and lambda at one horizontal level. A dental drill was used to create an opening of ~3 mm on the skull and the left primary auditory cortex was exposed. Throughout the surgery and experiments, the mouse body temperature was maintained at 37 °C using a feedback-controlled heating pad.

Acoustic stimulation

Pure tone bursts of 20 ms duration and 5 ms rising/decay time were used for acoustic stimulation. Digital sinusoid wave bursts were generated and converted to analog wave bursts by using a real-time processor (RP2; Tucker-Davis Tech. Inc., Gainesville, FL, USA). The analog signal was sent to a condenser loud speaker via a digitally controlled attenuator (PA5; Tucker-Davis) and a power amplifier. A flat frequency–response curve was sustained by using output signals from the RP2 that ranged from 9.2 to 20 V. The frequency and amplitude of tone bursts were either manually or automatically varied using Brainware software (Tucker-Davis). The condenser loud speaker was positioned 35 cm from and 45° right of the mouse right ear. The speaker output was calibrated using a Larson–Davis condenser microphone (Model 2520) and a microphone preamplifier (Model 2200C) and the tone intensity (at mouse right ear) was expressed as decibels sound pressure level (dB SPL, re. 20 μPa). Tone bursts were delivered to the mouse at a rate of 1 Hz when cortical responses to identical tone bursts were examined or at a rate of 4 Hz when cortical responses to a series of tone bursts with various frequencies and amplitudes were examined. For RF construction, a frequency–amplitude (FA) scan was used. For each FA scan, tone bursts were randomly varied from 3 to 40 kHz in frequency and from 0 to –100 dB in amplitude. A total of 798 FA blocks were used. An identical tone burst was presented ten times per FA block.

Recording of SPKs and LFPs in the left primary auditory cortex

A tungsten electrode or a multibarrel glass electrode with a carbon-fiber in the central tubing was used for recording neural activities in the primary auditory cortex. The impedance of the recording electrodes was approximately 1–2 MΩ. The multibarrel electrode was also used for drug microiontophoresis to the recording site (i.e. recorded neurons) as described below. The recording electrode was connected to a 16-channel preamplifier (PA16) and amplifier (RA16; both from Tucker-Davis). Bioelectrical signals were digitized in PA16 and then transferred to RA16 using an optical fiber.

In RA16, the signals were fed to two recording channels; one was amplified 10 000 times and filtered with a bandpass of 0.3–10 kHz for SPK recording and the other was amplified 1000 times and filtered with a bandpass of 1–200 Hz for LFP recording. The electrode was oriented perpendicularly to the auditory cortical surface for penetration. We typically made 5–8 electrode penetrations in each animal to confirm the placement of the electrode within the primary auditory cortex. Optimal neuronal responses to tone stimulation were usually recorded at a depth of about 300–600 μm below the brain surface (i.e. at layers III–IV). The original tracings from two recording channels were saved in DAM files using BrainWare data acquisition software (Tucker-Davis) for offline data processing.

Microniontophoretic injection of saline, muscimol and BMI

The multibarrel glass electrode with a tip diameter of 15–20 μm consisted of six glass tubes. Five glass barrels surrounded a central tube that contained a carbon-fiber connected to the PA16 preamplifier of the recording system (see above). Three of the surrounding barrels were filled with isotonic saline solution (0.9% NaCl, pH 7.0), one for grounding, one for balancing and one for saline injection. The remaining barrels were filled with either muscimol (a GABA_AR agonist, 9 mM, pH 6.47) or bicuculline methiodide (BMI, a GABA_AR antagonist, 10 mM, pH 3.0). The barrels were connected to the Neuro Phore System (BH-2; Harvard Apparatus, Inc., Holliston, MA, USA) for microiontophoretic injection of drugs. The injection current was +50 nA for muscimol, +50 nA for BMI and +50 nA for saline. A retention current of –30 nA for muscimol and –25 nA for BMI was applied to each drug-filled barrel during non-injection periods. Drug injections began after control data (RFs) were sampled and continued until RF data under drug impact were completed.

Data processing and statistical analysis

The original bioelectrical tracings (SPKs and LFPs) from the saved DAM files were analysed and processed by our custom-made software (SoundCode). Neuronal responses to the tone bursts and RFs obtained from the SPK and LFP data were compared.

SPK was defined as the action potential in which the amplitude was larger than a voltage-trigger level that was 1.2 times larger than the largest noise amplitude. We set this level to make it comparable with our LFP data (see below). We compared the RF_{SPK} using trigger voltage levels 1.2 and 2 times higher than the noise level. Excluding the clearly lower SPK numbers, the RF areas and bandwidths at the 1.2 times trigger level were similar to those at the 2 times trigger level. Our calculation utilized 3 times the standard deviation of the noise amplitude. Due to the stable noise level and large sample size, our calculated trigger level was lower than 1.2 times. Additionally, we examined the action potentials and field excitatory postsynaptic potentials (fEPSPs) of single cortical neurons using loose patch clamp recordings (impedance of the electrode tip was 15 MΩ). The RFs constructed on these action potentials and fEPSPs were mostly identical (data not shown). SPKs were sorted or isolated using a computer-based spike-sorting technique, i.e. using nine parameters of the SPK waveform: peak, peak time, peak duration, valley, valley time, valley duration, peak–valley amplitude, peak raising slope and peak–valley slope (Suga *et al.*, 1997; Yan & Ehret, 2002; Yan & Zhang, 2005; Luo *et al.*, 2008). Rasters and peri-stimulus time histograms (PSTs) or PST cumulative histograms (PSTCs) were plotted to display the responses of cortical neurons to tone stimuli. The binwidth of PSTs and PSTCs was 1 ms. The

auditory response magnitude of cortical neurons was the SPK number, i.e. the sum of all action potentials of cortical neurons in response to ten identical tone stimuli within a time frame of 10–60 ms from the onset of the tone bursts. The response latency was the time interval from the tone onset to the intersection point of the baseline to the rising slope of the PSTC.

LFPs were averaged waveforms based on ten tracings in response to ten identical tone stimuli. Cortical LFPs typically consisted of a negative-going wave followed by a positive-going wave. In this study, LFP amplitude and latency were measured based on the negative-going wave as the negative-going wave largely represents the assembly of thalamocortical fEPSPs. LFP amplitude was the micro-volt difference from the baseline to the peak of the negative-going wave within a time frame of 10–60 ms. LFP latency was the time interval from the tone onset to the intersection point of the baseline and slope of the negative-going wave.

RFs were visualized by plotting SPKs (raster, PSTs or PSTCs) and LFPs (averaged tracings) as a function of the tone frequencies and amplitudes (FA scan). RF area was defined by the response threshold curve of cortical neurons to single tone frequencies as described below.

For SPK data, the criteria for determining a threshold to a given frequency were the dB SPLs for which cortical neurons showed at least one spike more than the spike number without tone presentation. In addition, the spike numbers to both 5- and 10-dB levels below threshold needed to be lower than or equal to that without tone presentation (Suga *et al.*, 1997; Yan & Ehret, 2002; Yan & Zhang, 2005; Luo *et al.*, 2008). Based on these criteria, the thresholds to all frequencies were digitally analysed. The curve connecting the thresholds to all frequencies represented the frequency-threshold tuning curve, i.e. RF_{SPK} .

For LFP data, the criteria for determining a threshold to a given frequency were the dB SPLs to which LFP amplitude was larger than 1.2 times the voltage fluctuation without tone presentation. In addition, the LFP amplitudes to both 5- and 10-dB levels below threshold needed to be lower than or equal to 1.2 times the voltage fluctuation without tone presentation. The curve connecting the thresholds to all frequencies represented the frequency-threshold tuning curve, i.e. RF_{LFP} .

The RF was quantified with multiple parameters: BF, minimum threshold (MT), spike number (SPK)/amplitude (LFP) and latency at

10–20 dB above the MT, bandwidths (octaves) at 10, 30, 50 and 70 dB above the MT (BW10, BW30, BW50 and BW70) and RF areas below 30 and 50 dB SPL (RF_{30} and RF_{50}). The BF was the frequency (kHz) to which cortical neurons showed the lowest response threshold. The MT was the tone amplitude (dB SPL) to which cortical neurons showed the lowest response threshold across all frequencies. The BWs were the difference in octaves between the high- and low-frequency boundaries of RF measured at 10, 30, 50 and 70 dB above the MT. RF_{30} and RF_{50} were the number of frequency-amplitude blocks within RF below 30 and 50 dB SPL.

RF_{SPK} and RF_{LFP} were compared based on these RF parameters. All data were expressed as mean \pm SD. A Mann–Whitney U test was used to examine the significance of latency data differences. A paired *t*-test was used to examine the significance of other data differences between RF_{SPK} and RF_{LFP} and the changes in RF_{SPK} and RF_{LFP} before and after drug application. A *P* value of less than 0.05 was considered statistically significant.

Results

In total, multi-unit responses at 51 auditory cortex recording sites were sampled from 37 mice, and the RF_{SPK} and RF_{LFP} were compared. Of this group, multi-unit responses at 15 auditory cortex recording sites were recorded using the multibarrel electrode, seven for examining the muscimol (GABA_AR agonist) effects and eight for examining the BMI (GABA_AR antagonist) effects on the RF_{SPK} and RF_{LFP} of cortical neurons.

Examples of RF_{SPK} and RF_{LFP} recorded with the same electrode

Figure 1 shows an example of RF_{SPK} and RF_{LFP} sampled simultaneously using the same tungsten electrode. Tone-evoked spikes, as denoted by red dots that align because of relatively steady response latencies, exhibit a clear response area (i.e. RF_{SPK}). Obvious spontaneous spikes and spike bursts appeared outside of the RF_{SPK} area and their occurrences varied randomly in time. Tone-evoked LFPs (negative blue waveforms) superimposed on spikes are clear in all frequency–amplitude blocks within the RF_{SPK} area. At the boundary of the RF_{SPK} area, some blocks show negative-going waves with rare tone-evoked spikes. Outside the RF_{SPK} area, it is clear that

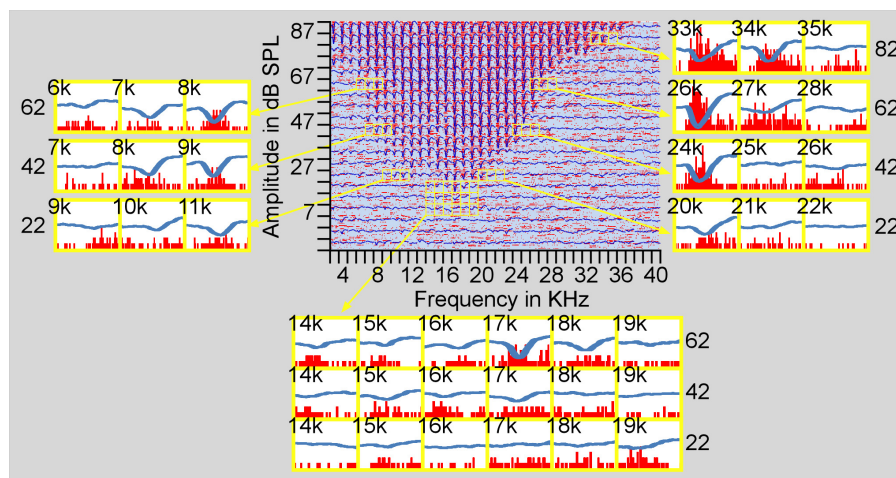


FIG. 1. Examples of the responses of auditory cortex neurons to tones of various frequencies and amplitudes. The central panel shows the raster of SPKs and averaged tracings of LFPs that are superimposed. The superimposed PSTs and LFTs from the MT boundaries are shown in the lower panel while those around 10, 30, 50 and 70 dB above MT are shown in the left and right panels.

spontaneous spikes and/or spike bursts were not accompanied by LFPs. The BFs based on both RF_{SPK} and RF_{LFP} were 17 kHz. The MT of RF_{SPK} was 30 dB SPL and that of RF_{LFP} was 25 dB SPL, 5 dB lower than RF_{SPK} MT.

The RF boundary region of this sample is further illustrated by the PSTs that overlapped with LFPs around the MT, both sides of the RF at 10, 30 and 50 dB above the MT, and the high-frequency side at 70 dB above the MT. Around the MT area (Fig. 1, lower panel), tone-evoked spikes are visualized at the block 17 kHz/30 dB SPL (17/30 block) but not at the 17/25 and 17/20 blocks. Tone-evoked LFPs can be identified at the 17/30 and 17/25 blocks. At blocks 14/30, 15/30, 16/30, 18/30, 15/25, 16/25 and 19/20, spikes that were spontaneous or evoked by tone stimuli cannot be visually confirmed. Based on our criteria, these blocks were not included in the RF_{SPK} area. At these blocks, however, tone-evoked LFPs are identifiable. The remaining blocks in the lower panel show neither tone-evoked spikes nor LFPs. At the low-frequency side of RF_{SPK} area (Fig. 1, left panel), tone-evoked spikes and LFPs appear at blocks 7/75, 6/75, 8/55 and 7/55. Tone-evoked LFPs also appear at blocks 5/75, 11/35 and 10/35 in which tone-evoked spikes are unclear. At the high-frequency side (Fig. 1, right panel), LFPs appear only at the blocks in which tone-evoked spikes are clear.

These examples demonstrate a similarity in the size of RF_{SPK} and RF_{LFP}. The RF_{LFP} was slightly larger than the RF_{SPK}, particularly at lower tone levels.

Similar BFs and MTs of RF_{SPK} and RF_{LFP}

The RF_{SPK} BFs of our samples ranged from 10 to 25 kHz (17.31 ± 3.43 kHz), which was not significantly different ($n = 51$, $P > 0.05$) from the RF_{LFP} BFs that ranged from 9 to 24 kHz (17.02 ± 3.36 kHz). The BFs measured based on RF_{SPK} and RF_{LFP} were highly correlated (slope = 0.88, $r = 0.81$, $P < 0.001$, Fig. 2A1). The RF_{LFP} BFs could be either higher or lower than the RF_{SPK} BFs but the difference was < 5 kHz. Of 51 samples, 23 (45.09%) neurons had identical BFs, 19 (37.25%) had a 1-kHz difference, five (9.8%) had a 2-kHz difference and four (7.8%) had a > 2 -kHz difference between RF_{SPK} and RF_{LFP} (Fig. 2A2). The RF_{SPK} MTs ranged from -0.76 to 32.1 dB SPL, 13.70 ± 6.67 dB SPL, which was significantly higher than the RF_{LFP} MTs that ranged from -0.76 to 31.7 dB SPL, 11.88 ± 6.63 dB SPL ($n = 51$, $P < 0.001$). The MTs of RF_{SPK} and RF_{LFP} were also correlated (slope = 0.96, $r = 0.88$, $P < 0.001$, Fig. 2B1). The RF_{LFP} MTs were either equal to (31 neurons, 60.78%) or ~ 5 dB lower than (20 neurons, 39.22%) the RF_{SPK} MTs (Fig. 2B2). The BFs and MTs of the sampled neurons fell within the central range of C57 mouse hearing.

Correlations of latency and magnitude of spikes and LFPs in response to tone stimuli

In most cases, response latencies measured from SPK data were longer than those from LFP data. On average, SPK latencies were 27.17 ± 5.78 ms at 10 dB above the MT and 23.75 ± 6.32 ms at 20 dB above the MT. LFP latencies were 21.59 ± 3.55 ms at 10 dB above the MT and 18.29 ± 3.32 ms at 20 dB above the MT. SPK latencies were significantly longer than LFP latencies at both 10 dB ($n = 51$, $P < 0.001$) and 20 dB ($n = 51$, $P < 0.001$) above the MT. The average differences in latencies between SPK and LFP were 6.47 ± 4.03 ms at 10 dB and 5.46 ± 4.44 ms at 20 dB above the MT. As shown in Fig. 2C, the SPK and LFP latencies were linearly correlated to each other at both 10 dB

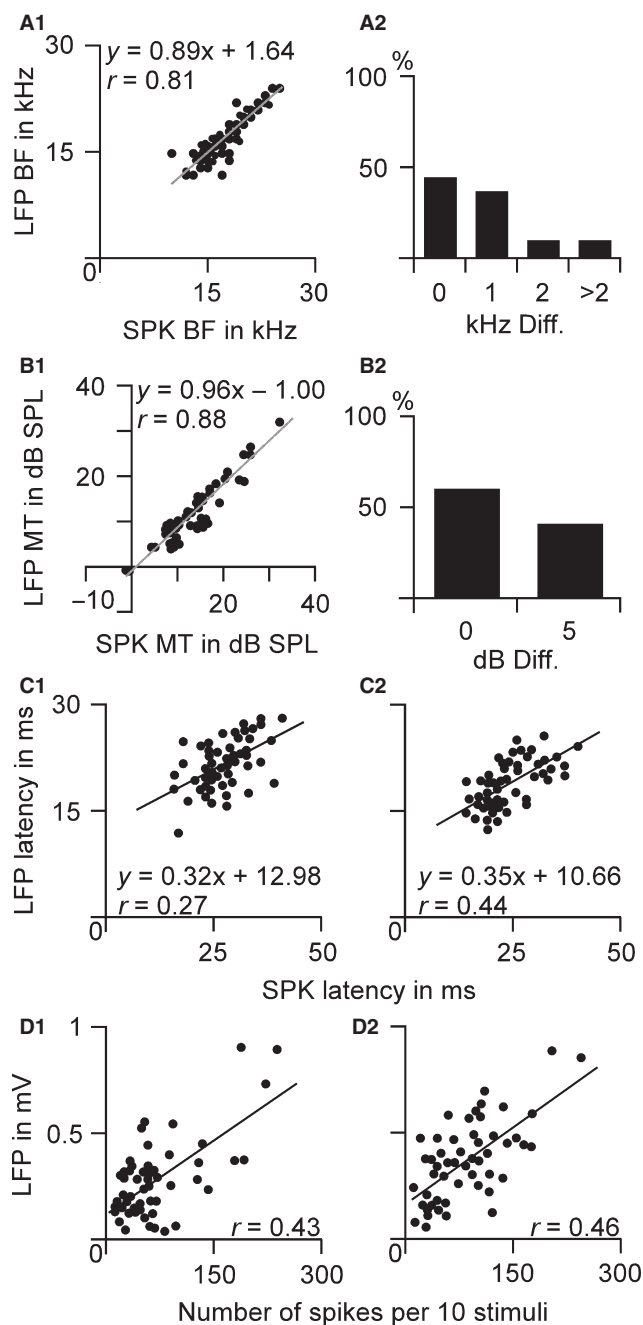


FIG. 2. Comparisons of RF_{SPK} and RF_{LFP}. The BFs (A1) and MTs (B1) of RF_{SPK} and RF_{LFP} were highly correlated and their differences were small, a few kHz difference in BFs (A2) and < 5 dB in MTs (B2). Their response latencies and magnitudes at 10 dB (C1 and D1) and 20 dB (C2 and D2) above the MT were also correlated.

(Fig. 2C1, $r = 0.27$, $P = 0.055$) and 20 dB (Fig. 2C2, $r = 0.44$, $P < 0.01$) above the MT.

The response magnitudes were expressed by SPK number and LFP amplitude in response to BF tones at 10 and 20 dB above the MT. SPK numbers were 70.71 ± 54.31 in response to tones at 10 dB above MT and 84.08 ± 51.64 at 20 dB above MT ($n = 51$). LFP amplitudes were 281.49 ± 194.53 μ V in response to tones at 10 dB above MT and 364.84 ± 188.11 μ V at 20 dB above MT ($n = 51$). SPK response magnitudes were linearly correlated to the LFP ones at both tone levels 10 dB (Fig. 2D1, $r = 0.43$, $P < 0.01$) and 20 dB (Fig. 2D2, $r = 0.46$, $P < 0.001$) above the MT.

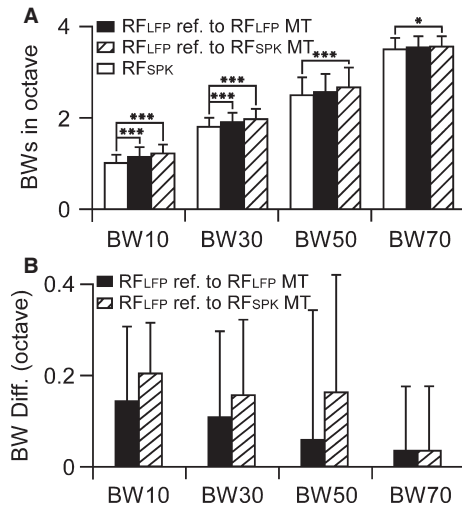


FIG. 3. Comparisons of RF_{SPK} and RF_{LFP} BWs. The BW increased (A) and BW differences gradually decreased (B) in response to the increases in tone level. * $P < 0.05$, *** $P < 0.001$.

Correlations of bandwidths and areas of RF_{SPK} and RF_{LFP}

The shapes of RF_{SPK} and RF_{LFP} were similar; RF_{LFP} appeared slightly larger than RF_{SPK} as shown in Fig. 1. We compared the frequency BWs of RF_{SPK} and RF_{LFP} at 10, 30, 50 and 70 dB above the MT. All BWs of RF_{SPK} were narrower than those of RF_{LFP}. The statistically significant narrowing was found at lower tone levels only (Fig. 3A, open and filled columns), i.e. BW10 ($P < 0.001$) and BW30 ($P < 0.05$). As many MTs of RF_{LFP} were lower than those of RF_{SPK}, we used RF_{SPK} MT as a reference point to measure and compare the BWs of RF_{SPK} and RF_{LFP}. The RF_{LFP} BWs measured at 10, 30, 50 and 70 dB above the RF_{SPK} MTs were broader than those above RF_{LFP} MTs (Fig. 3, filled and hatched columns). Compared with the RF_{SPK} BWs, RF_{LFP} BWs referred to RF_{SPK} MTs were significantly broader at all four levels (Fig. 3, open and hatched columns), i.e. BW10 ($P < 0.001$), BW30 ($P < 0.001$), BW50 ($P < 0.001$) and BW70 ($P < 0.05$).

The RF_{LFP} BWs were commonly several kilohertz wider than RF_{SPK} BWs (Fig. 3B). At higher tone levels, RF_{LFP} BWs (such as BW50 and BW70) were not different from RF_{SPK} BWs in many neurons. When RF_{LFP} BWs were referred to RF_{LFP} MTs, the differences of RF_{LFP} and RF_{SPK} were 0.14 ± 0.17 octaves (oct) for BW10, 0.11 ± 0.19 oct for BW30, 0.06 ± 0.28 oct for BW50 and 0.03 ± 0.11 oct for BW70 ($n = 51$, Fig. 3B, filled column). When RF_{LFP} BWs were referred to RF_{SPK} MTs, the differences of RF_{LFP} and RF_{SPK} were 0.21 ± 0.12 oct for BW10, 0.16 ± 0.17 oct for BW30, 0.17 ± 0.25 oct for BW50 and 0.03 ± 0.11 oct for BW70 ($n = 51$, Fig. 3B, hatched column). The differences in BWs between RF_{SPK} and RF_{LFP} were negatively related to the tone level.

We further analysed the areas between RF_{SPK} and RF_{LFP} below 30 dB SPL (RF30) and 50 dB SPL (RF50). As expected based on the differences in MTs and BWs, the RF30 and RF50 of RF_{SPK} were smaller than those of RF_{LFP}. RF30 was 57.15 ± 21.53 kHz \times 5 dB for RF_{SPK} and 69.96 ± 24.64 kHz \times 5 dB for RF_{LFP}; these results were significantly different ($n = 51$, $P < 0.001$) and linearly correlated (Fig. 4A). The RF50 of RF_{SPK}, 142.54 ± 34.05 kHz \times 5 dB, was also significantly smaller than that of RF_{LFP}, 162.37 ± 37.69 kHz \times 5 dB ($n = 51$, $P < 0.001$), and also linearly correlated (Fig. 4B). On average, the RF30 of RF_{SPK} was $17.25 \pm 12.18\%$ smaller than that of RF_{LFP} and RF50 was $11.63 \pm 6.23\%$ smaller.

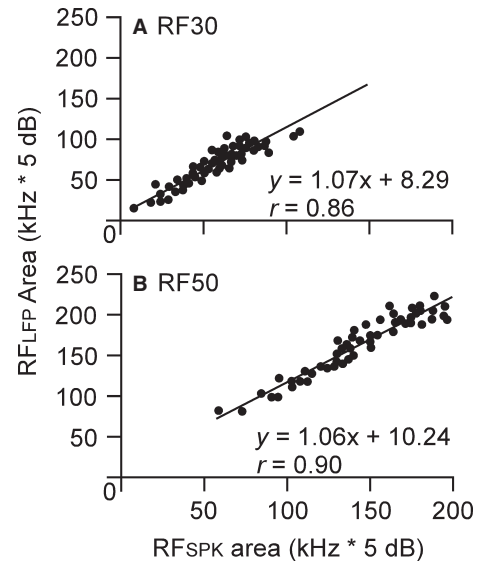


FIG. 4. Comparisons of RF_{SPK} and RF_{LFP} areas below 30 dB SPL (A) and 50 dB SPL (B).

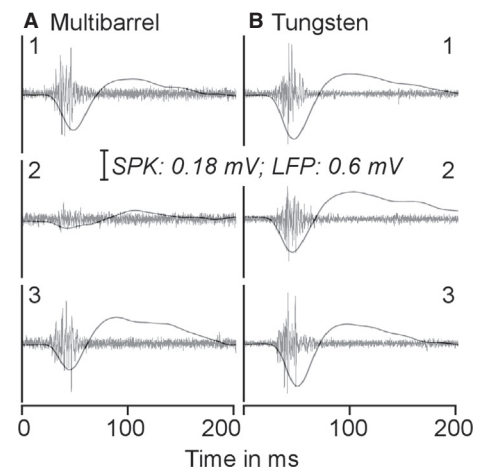


FIG. 5. An example of the effect of muscimol microiontophoresis on the auditory responses of auditory cortex neurons recorded with a multibarrel electrode (A) and a tungsten electrode (B) separated by about 100 μ m in placement. Neurons recorded by the two electrodes showed vigorous responses to tones at BF and 20 dB above the MT (A1 and B1). Muscimol application to the neurons in A drastically reduced the auditory responses of the neurons in A (A2) but only slightly reduced the auditory responses of the neurons in B (B2). The changes in both SPK and LFP were closely related (A1–2 and B1–2). The auditory responses recovered 26 min after the cessation of muscimol microiontophoresis are also shown (A3 and B3).

Effects of cortical inhibition at the muscimol microiontophoretic site and the remote site

We next examined the effects of microiontophoretic injection of muscimol on auditory responses of cortical neurons recorded by a multibarrel electrode (injection site) and a tungsten electrode placed about ~ 100 μ m apart from each other (non-injection site). Auditory responses were induced by a tone at the BF and 20 dB above the MT of the auditory cortex neurons recorded by the multibarrel electrode. A pair of examples is shown in Fig. 5; both auditory cortex sites recorded by the multibarrel and tungsten electrodes tuned to 16 kHz and had similar RFs. At 20 dB above the MT, the

microiontophoresis of muscimol largely reduced the response magnitudes (both SPK and LFP) recorded by the multibarrel electrode but only slightly reduced those recorded by the tungsten electrode (Fig. 5A1–2 and B1–2). Neuronal responses returned 41 min after cessation of the muscimol application (Fig. 5A3 and B3). In total, seven pairs of samples were recorded in seven mice. Of seven samples recorded with the multibarrel electrodes, the auditory responses (SPK and LFP) of three samples were completely eliminated and those of four neurons were largely reduced as shown in Fig. 5A1. The auditory responses of seven samples recorded by the tungsten electrode (about 100 μm from the site of the muscimol application) were slightly reduced. The changes in SPK number and LFP amplitude were synchronous.

For the seven samples recorded by the multibarrel electrode, muscimol application reduced their SPK number from 81.43 ± 17.39 to 15.57 ± 15.50 (a 80.89% decrease, $P < 0.001$) and their LFP amplitude from 404.14 ± 180.86 to 54.43 ± 60.68 μV (an 81.60% decrease, $P < 0.005$). For the seven samples recorded by the tungsten electrode, muscimol application reduced their SPK number from 97.29 ± 61.58 to 68.29 ± 48.12 (a 34.85% decrease, $P < 0.01$) and their LFP amplitude from 429.43 ± 266.43 to 260.86 ± 153.02 μV (a 37.01% decrease, $P < 0.05$). In three samples recorded by the multibarrel electrode, their auditory responses were completely eliminated by muscimol. The extent of the decreased auditory responses in their counterparts recorded by the tungsten electrode was small, 40.39% for SPK and 37.40% for LFP. In terms of percentage changes, there were no differences between SPK numbers and LFP amplitudes. The percentage decreases in both SPK and LFP were significantly larger in samples recorded by the multibarrel electrode than in those recorded by the tungsten electrode ($n = 7$, $P < 0.005$ for SPK and $P < 0.05$ for LFP).

Effects of cortical BMI on cortical RF_{SPK} and RF_{LFP}

The microiontophoresis of BMI in the vicinity of the electrode tip disinhibited the recorded neurons. Sampled multi-units showed obvious increases in response magnitudes including SPK number and LFP magnitude while slightly broadening their RF BWs. The changes induced by BMI application were very similar in RF_{SPK} and RF_{LFP} (Fig. 6). We obtained eight samples from eight mice. BMI microiontophoresis increased SPK number by $165.52 \pm 129.20\%$, from 74.12 ± 28.25 to 182.25 ± 67.55 ($P < 0.001$) while broadening the overall BW (sum of BW10–50) by only $11.42 \pm 10.35\%$, from 1.78 ± 0.67 to 2.03 ± 0.76 oct ($P < 0.01$). Similar results were seen with the LFP data. BMI microiontophoresis increased LFP magnitude by $160.36 \pm 130.89\%$, from 372.25 ± 210.64 to 759.38 ± 190.27 μV ($P < 0.001$) while broadening the overall BW by only $10.09 \pm 11.14\%$, from 1.89 ± 0.64 to 2.07 ± 0.71 oct ($P < 0.01$). No statistical differences were found in the percentage changes in both the response magnitudes and BWs between RF_{SPK} and RF_{LFP} ($P > 0.05$).

Discussion

Extracellular field potentials in the brain are directly associated with proximate neural activities. The composition of the bioelectrical signals obtained through extracellular recording with a high-impedance electrode originates from various neural processes (Cole, 1968; Freeman & Stone, 1969; Martin, 1976; Mitzdorf, 1985; Borg-Graham *et al.*, 1998; Noreña & Eggermont, 2002; Metherate *et al.*, 2004; Gieselmann & Thiele, 2008; Kajikawa & Schroeder, 2011; de Cheveigné *et al.*, 2013). Two important neural components, LFP

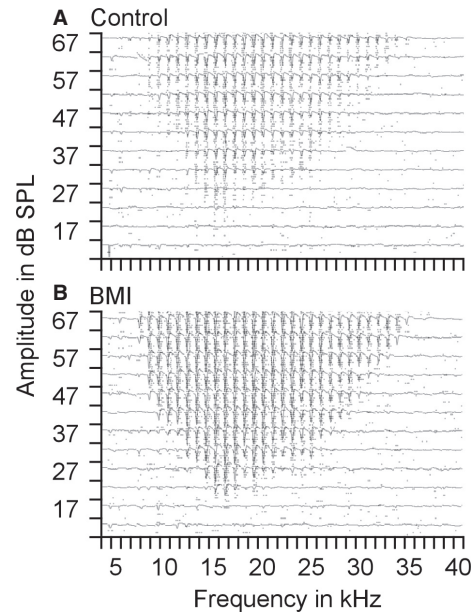


FIG. 6. Examples of the responses of auditory cortex neurons to tones of various frequencies and amplitudes before (A) and after (B) microiontophoresis of BMI. The raster of SPK (dots) and superimposed averaged tracings of LFP (traces) are shown. BMI application slightly enlarged the excitatory response area but greatly increased the response magnitude.

and SPK, have been used for the investigation of neural functions at the systems level. LFP is a low-frequency voltage fluctuation (less than ~ 300 Hz) that is believed to mostly represent the integrated EPSPs (Gustafsson, 1984; Mitzdorf, 1985; Buzsáki & Kandel, 1998; Schroeder *et al.*, 1998; Galván *et al.*, 2001; Logothetis, 2003; Nunez, 2006; Kurt *et al.*, 2007; Berens *et al.*, 2008; Eggermont *et al.*, 2011; Lindén *et al.*, 2011). Extracellular signals sorted by different frequency filter settings help to differentiate the input (LFP) and output (SPK) of cortical neurons, providing a unique tool to probe the dynamics of cortical local circuitry (Lorente de No, 1947; Eccles, 1951; Eggermont, 1996; Chrobak & Buzsáki, 1998; Buzsáki & Draguhn, 2004; Metherate *et al.*, 2004; Lakatos *et al.*, 2005; Mormann *et al.*, 2005; Canolty *et al.*, 2006; Einevoll *et al.*, 2007; Katzner *et al.*, 2009; Denker *et al.*, 2010, 2011; Kelly *et al.*, 2010; Eggermont *et al.*, 2011).

Anatomical investigations using the rabbit model have demonstrated that a single thalamocortical neuron is capable of innervating a large cortical area. In other words, a single cortical neuron may receive inputs from many thalamocortical neurons (De Venecia & McMullen, 1994). Theoretically, the RFs or spectral ranges of cortical neurons should be much broader than those of thalamocortical neurons. It is understood that the spectral range measured on neuronal spikes in the cat auditory cortex is not dramatically broader than that in the auditory thalamus (Calford *et al.*, 1983; Miller *et al.*, 2001, 2002). The misalignment of anatomical and physiological findings is reconciled by the comparison of cortical SPK and LFP RFs in various species including cats, guinea pigs and monkeys. These studies confirm that the RFs or frequency tunings of cortical neurons constructed on LFPs are much broader than those constructed on SPKs (monkey visual cortex: Buracas *et al.*, 1998; cat cortex: Miller *et al.*, 2002; Noreña & Eggermont, 2002; rat cortex: Wehr & Zador, 2005). The findings suggest that the output of cortical neurons are extensively shaped by intracortical neural circuits, i.e. the inhibitory processing through GABA_ARs (Hirsch *et al.*, 1998; Muller & Scheich, 1988; Wang *et al.*, 2000, 2002;

Foeller *et al.*, 2001; Noreña & Eggermont, 2002; Wehr & Zador, 2005; Eggermont *et al.*, 2011; de Cheveigné *et al.*, 2013).

In this study, we compared the RF_{SPK} and RF_{LFP} recorded by the same electrode in the primary auditory cortex of mouse. We have shown that the shapes of the RF_{SPK} and RF_{LFP} were similar (Fig. 1); the BFs, MTs, BWs and RF sizes of the RF_{SPK} and RF_{LFP} were highly correlated (Figs 2–4). The RF_{SPK} BF could be higher, lower or equal to RF_{LFP} BF from neuron to neuron but there were no significant differences between them. In contrast, the RF_{SPK} MTs were never lower than RF_{LFP} MTs; RF_{SPK} MTs were significantly higher than RF_{LFP} MTs. For the most part, the RF_{SPK} BWs were narrower than RF_{LFP} BWs. This close correspondence between RF_{SPK} and RF_{LFP} could be a specific feature of the mouse auditory cortex.

Our findings in mice are generally in line with previous findings with some notable differences. First, the difference in spectral ranges between RF_{SPK} and RF_{LFP} are much smaller than those observed in large animals. The RF_{LFP} BW can be two to three times the RF_{SPK} BW in cats (Noreña & Eggermont, 2002), guinea pigs (Gaucher *et al.*, 2012; de Cheveigné *et al.*, 2013) and monkeys (Kajikawa & Schroeder, 2011). Our data revealed that the RF_{LFP} BW was only about 10% wider than the RF_{SPK} BW (Fig. 3B) in C57 mice; this 10% could be more significant due to the measurement on a linear scale. This difference is particularly interesting because the absolute area of the auditory cortex is smaller but the range of spectral representation is wider in the mouse. Secondly, the differences in RF size and spectral range appeared to depend on sound levels. The higher the tone level, the smaller the differences of BWs were between RF_{SPK} and RF_{LFP} (Fig. 3B). Statistically significant data were reported at BW10 and BW30 only (Fig. 3). This level-dependence was also indicated by the comparative results at RF30 and RF50. RF_{SPK} size was $17.25 \pm 12.18\%$ smaller than RF_{LFP} size below 30 dB SPL while RF_{SPK} size was $11.63 \pm 6.23\%$ smaller than RF_{LFP} size below 50 dB SPL.

Cortical LFP is considered a focal bioelectrical signature of neuronal activity that is closely correlated to functional magnetic resonance imaging and electroencephalography signals. Despite being an ‘ancient’ technique, measuring the LFP remains a valuable and widely used tool for investigating the neural mechanisms of cortical sensory processing and behaviors (Kreiman *et al.*, 2006; Liu & Newsome, 2006). Stimulus-evoked cortical LFP is understood to represent the assembly of EPSPs of cortical recipient layers. The broadness of RF_{LFP} area to RF_{SPK} area represents neuronal subthreshold activities.

A problematic issue is that the cortical region contributing to the LFP appears large in scale, varying from hundreds of microns to a few millimeters depending on the approach (Destexhe *et al.*, 1999; Kreiman *et al.*, 2006; Katzner *et al.*, 2009; Xing *et al.*, 2009). An important dispute remains the origin of the LFP, specifically if the cortical LFP is contaminated by unrelated electrical signals from a remote region (Katzner *et al.*, 2009; Eggermont *et al.*, 2011; Kajikawa & Schroeder, 2011; Lindén *et al.*, 2011; Gaucher *et al.*, 2012). The key issue here is not the size of the cortical region but whether the cortical LFP component from its more remote origins is the result of neural conduction or volume conduction. If it is the result of neural conduction, the remote component of LFP is actually a local event and a feature of neural integration of the recorded neurons. If it is the result of volume conduction, the remote component is probably a contaminated recording of the LFP. This clarification is important because direct evidence for contamination could greatly reduce the value of LFP as a tool for measuring the function of neural circuits. Previous studies with different techniques were unable to offer a definitive conclusion (Katzner *et al.*, 2009; Egger-

mont *et al.*, 2011; Kajikawa & Schroeder, 2011; Lindén *et al.*, 2011; Gaucher *et al.*, 2012; Einevoll *et al.*, 2013).

The primary auditory cortex surface of the C57 mouse is about $2 \times 1 \text{ mm}^2$ and its spectral range spans up to 40 kHz (Zhang *et al.*, 2005; Luo *et al.*, 2009). This suggests that the frequency maps or representations in the mouse auditory cortex are denser than those in cats, guinea pigs and monkeys. If the broader frequency range of RF_{LFP} is the result of volume conduction, the broadness of the frequency range (i.e. BWs) of RF_{LFP} to RF_{SPK} in mouse would need to be much greater than those found in larger animals. Our data showed the reverse. As described above, the BWs of RF_{LFP} were only slightly wider than those of RF_{SPK} and the broadness of RF_{LFP} were even more significant at lower sound levels. Based on these findings, it is clear that the broader RF_{LFP} cannot include the components of remote bioelectrical signals through volume conduction. Instead, it appears to represent the subthreshold alteration of membrane potentiation (Kaur *et al.*, 2004; Berens *et al.*, 2008; Eggermont *et al.*, 2011). This conclusion is corroborated by our paired recordings from the multibarrel and tungsten electrodes. When SPKs and LFPs were largely or completely eliminated by focal application of muscimol (a GABA_AR agonist) to the recorded neurons, the SPKs and LFPs of neighboring neurons (~100 μm apart) were reduced by < 50%. If this <50% deduction is considered to result from drug diffusion, the volume conduction can be excluded. However, if the diffusing impact of administered muscimol can be excluded (Fig. 5B2), these findings suggest that neural activities recorded by the tungsten electrode appear to contain the components of bioelectrical signals at remote sites where the multibarrel electrode was positioned. In other words, the neuronal activities of given neuron clusters may impact on the SPKs and LFPs within at least a 100- μm range. Most importantly, this impact was unidirectional because the SPK and LFP could be largely and even completely eliminated at the sites where muscimol was applied (Fig. 5B2) but not at the site ~100 μm away (Fig. 5B2). As physical propagation (e.g. volume conduction) of bioelectrical signals has no directional preference, the unidirectional impact of neural activities of neighboring recording sites (Fig. 5) indicates that the remote signals were transmitted through local neural circuits. Our data therefore suggest that the remote signals of cortical LFPs are the integrative components of a local event but also represent the contribution of neurons from distant sites.

In conclusion, this study demonstrates that the differences in the BWs between RF_{LFP} and RF_{SPK} were much smaller than those observed in large animals. Does this mean that the inhibitory process is much weaker in the mouse auditory cortex particularly when volume conduction can be excluded? Our data further showed that the microiontophoresis of the GABA_AR antagonist BMI increased SPK number and LFP amplitude by more than 160% while broadening BWs of RF_{SPK} and RF_{LFP} by about 10% only (Fig. 6). These findings suggest that the GABA-mediated inhibitory processing in the mouse auditory cortex appears as strong as those in cats, guinea pigs and monkeys but its contribution to the sharpening of RF_{SPK} is relatively small. Note that a study in rodents indicates that BMI has little impact on tuning broadening, probably due to BMI effects on calcium-dependent potassium channels (a non-GABAergic effect; Kurt *et al.*, 2006). If viewed in the context of our muscimol data, the conclusion that lateral excitation contributes to a spectral range of cortical neurons is a viable possibility. A similar degree of broadening of RF_{SPK} and RF_{LFP} induced by the GABA_AR antagonist appears to support the original assumption that the broader portion of cortical LFP depicts the subthreshold fEPSPs of thalamocortical inputs.

Supporting Information

Additional supporting information can be found in the online version of this article:

Fig. S1. The comparison of the receptive fields constructed on spikes that were isolated by using trigger levels 1.2 times and 2 times higher than the noise level.

Fig. S2. Example of the receptive fields constructed on action potentials and fEPSPs of single neurons recorded by the same glass electrode (loose patch recording).

Acknowledgements

We are grateful to Dr Jos J. Eggermont for his comments on this article. This work was supported by grants from the Canadian Institutes of Health Research (MOP164961, MOP274494), the Natural Sciences and Engineering Research Council of Canada (DG261338-2009), Alberta Innovates – Health Solutions and the Campbell McLaurin Chair for Hearing Deficiencies, University of Calgary.

Abbreviations

BF, best frequency; BMI, bicuculline methiodide; BW, bandwidth; FA, frequency–amplitude; fEPSP, field excitatory postsynaptic potential; GABA_AR, γ -aminobutyric acid receptor A; LFP, local field potential; MT, minimum threshold; PST, peri-stimulus time histogram; PSTC, peri-stimulus cumulative histogram; RF, receptive field; SPK, spike activity.

References

Barkat, T.R., Polley, D.B. & Hensch, T.K. (2011) A critical period for auditory thalamocortical connectivity. *Nat. Neurosci.*, **14**, 1189–1194.

Berens, P., Keliris, G.A., Ecker, A.S., Logothetis, N.K. & Tolias, A.S. (2008) Feature selectivity of the gamma-band of the local field potential in primate primary visual cortex. *Front. Neurosci.*, **2**, 199–207.

Borg-Graham, L.J., Monier, C. & Frégnac, Y. (1998) Visual input evokes transient and strong shunting inhibition in visual cortex neurons. *Nature*, **393**, 369–373.

Buracas, G.T., Zador, A.M., DeWeese, M.R. & Albright, T.D. (1998) Efficient discrimination of temporal patterns by motion-sensitive neurons in primate visual cortex. *Neuron*, **20**, 959–969.

Buzsáki, G. & Draguhn, A. (2004) Neuronal oscillations in cortical networks. *Science*, **304**, 1926–1929.

Buzsáki, G. & Kandel, A. (1998) Somadendritic backpropagation of action potentials in cortical pyramidal cells of the awake rat. *J. Neurophysiol.*, **79**, 1587–1591.

Calford, M.B., Webster, W.R. & Semple, M.M. (1983) Measurement of frequency selectivity of single neurons in the central auditory pathway. *Hearing Res.*, **11**, 395–401.

Canolty, R.T., Edwards, E., Dalal, S.S., Soltani, M., Nagarajan, S.S., Kirsch, H.E., Berger, M.S., Barbaro, N.M. & Knight, R.T. (2006) High gamma power is phase-locked to theta oscillations in human neocortex. *Science*, **313**, 1626–1628.

de Cheveigné, A., Edeline, J.M., Gaucher, Q. & Gourévitch, B. (2013) Component analysis reveals sharp tuning of the local field potential in the guinea pig auditory cortex. *J. Neurophysiol.*, **109**, 261–272.

Chrobak, J.J. & Buzsáki, G. (1998) Gamma oscillations in the entorhinal cortex of the freely behaving rat. *J. Neurosci.*, **18**, 388–398.

Cole, K.S. (1968) *Membranes, Ions and Impulses*. University of California Press, Berkeley, CA.

De Venecia, R.K. & McMullen, N.T. (1994) Single thalamocortical axons diverge to multiple patches in neonatal auditory cortex. *Dev. Brain Res.*, **81**, 135–142.

Denker, M., Riehle, A., Diesmann, M. & Grun, S. (2010) Estimating the contribution of assembly activity to cortical dynamics from spike and population measures. *J. Comput. Neurosci.*, **29**, 599–613.

Denker, M., Roux, S., Linden, H., Diesmann, M., Riehle, A. & Grun, S. (2011) The local field potential reflects surplus spike synchrony. *Cereb. Cortex*, **21**, 2681–2695.

Destexhe, A., Contreras, D. & Steriade, M. (1999) Spatiotemporal analysis of local field potentials and unit discharges in cat cerebral cortex during natural wake and sleep states. *J. Neurosci.*, **19**, 4595–4608.

Eccles, J.C. (1951) Interpretation of action potentials evoked in the cerebral cortex. *Electroen. Clin. Neuro.*, **3**, 449–464.

Eggermont, J.J. (1996) How homogeneous is cat primary auditory cortex? Evidence from simultaneous single-unit recordings. *Audit. Neurosci.*, **2**, 79–96.

Eggermont, J.J. (1998) Representation of spectral and temporal sound features in three cortical fields of the cat. Similarities outweigh differences. *J. Neurophysiol.*, **80**, 2743–2764.

Eggermont, J.J., Munguia, R., Pienkowski, M. & Shaw, G. (2011) Comparison of LFP-based and SPK-based spectro-temporal receptive fields and cross-correlation in cat primary auditory cortex. *PLoS One*, **5**, e20046.

Einevoll, G.T., Pettersen, K.H., Devor, A., Ulbert, I., Halgren, E. & Dale, A.M. (2007) Laminar population analysis: estimating firing rates and evoked synaptic activity from multielectrode recordings in rat barrel cortex. *J. Neurophysiol.*, **97**, 2174–2190.

Einevoll, G.T., Kayser, C., Logothetis, N.K. & Panzeri, S. (2013) Modelling and analysis of local field potentials for studying the function of cortical circuits. *Nat. Rev. Neurosci.*, **14**, 770–785.

Fiser, J., Chiu, C. & Weliky, M. (2004) Small modulation of ongoing cortical dynamics by sensory input during natural vision. *Nature*, **431**, 573–578.

Foeller, E., Vater, M. & Kossel, M. (2001) Laminar analysis of inhibition in the gerbil primary auditory cortex. *JARO*, **2**, 279–296.

Freeman, J.A. & Stone, J. (1969) A technique for current source density analysis of field potentials and its application to the frog cerebellum. In Llinas, R. (Ed.), *Neurobiology of Cerebellar Evolution and Development*. American Medical Association, Chicago, IL, pp. 421–430.

Galván, V.V., Chen, J. & Weinberger, N.M. (2001) Long-term frequency tuning of local field potentials in the auditory cortex of the waking guinea pig. *JARO*, **2**, 199–215.

Gaucher, Q., Edeline, J.M. & Gourévitch, B. (2012) How different are the local field potentials and spiking activities? Insights from multielectrode arrays. *J. Physiol.*, **106**, 93–103.

Gieselmann, M.A. & Thiele, A. (2008) Comparison of spatial integration and surround suppression characteristics in spiking activity and the local field potential in macaque V1. *Eur. J. Neurosci.*, **28**, 447–459.

Gustafsson, B. (1984) Afterpotentials and transduction properties in different types of central neurones. *Arch. Ital. Biol.*, **122**, 17–30.

Hackett, T.A., Barkat, T.R., O'Brien, B.M., Hensch, T.K. & Polley, D.B. (2011) Linking topography to tonotopy in the mouse auditory thalamocortical circuit. *J. Neurosci.*, **31**, 2983–2995.

Happel, M.F., Jeschke, M. & Ohl, F.W. (2010) Spectral integration in primary auditory cortex attributable to temporally precise convergence of thalamocortical and intracortical input. *J. Neurosci.*, **30**, 11114–11127.

Hirsch, J.A. (2003) Synaptic physiology and receptive field structure in the early visual pathway of the cat. *Cereb. Cortex*, **13**, 63–69.

Hirsch, J.A., Alonso, J.M., Reid, R.C. & Martinez, L.M. (1998) Synaptic integration in simple striate cortical simple cells. *J. Neurosci.*, **18**, 9517–9528.

Kajikawa, Y. & Schroeder, C.E. (2011) How local is the local field potential? *Neuron*, **72**, 847–858.

Katzner, S., Nauhaus, I., Benucci, A., Bonin, V., Ringach, D.L. & Carandini, M. (2009) Local origin of field potentials in visual cortex. *Neuron*, **61**, 35–41.

Kaur, S., Lazar, R. & Metherate, R. (2004) Intracortical pathways determine breadth of subthreshold frequency receptive fields in primary auditory cortex. *J. Neurophysiol.*, **91**, 2551–2567.

Kelly, R.C., Smith, M.A., Kass, R.E. & Lee, T.S. (2010) Local field potentials indicate network state and account for neuronal response variability. *J. Comput. Neurosci.*, **29**, 567–579.

Kenet, T., Bibitchkov, D., Tsodyks, M., Grinvald, A. & Arieli, A. (2003) Spontaneously emerging cortical representations of visual attributes. *Nature*, **425**, 954–956.

Kreiman, G., Hung, C.P., Kraskov, A., Quiroga, R.Q., Poggio, T. & DiCarlo, J.J. (2006) Object selectivity of local field potentials and spikes in the macaque inferior temporal cortex. *Neuron*, **49**, 433–445.

Kurt, S., Crook, J.M., Ohl, F.W., Scheich, H. & Schulze, H. (2006) Differential effects of iontophoretic in vivo application of the GABA_A-antagonists bicuculline and gabazine in sensory cortex. *Hearing Res.*, **212**, 224–235.

- Kurt, S., Moeller, C.K., Jeschke, M. & Schulze, H. (2007) Differential effects of iontophoretic application of the GABAA-antagonists bicuculline and gabazine on tone-evoked local field potentials in primary auditory cortex: interaction with ketamine anesthesia. *Brain Res.*, **1220**, 58–69.
- Kyriazi, H.T. & Simons, D.J. (1993) Thalamocortical response transformations in simulated whisker barrels. *J. Neurosci.*, **13**, 1601–1615.
- Lakatos, P., Shah, A.S., Knuth, K.H., Ulbert, I., Karmos, G. & Schroeder, C.E. (2005) An oscillatory hierarchy controlling neuronal excitability and stimulus processing in the auditory cortex. *J. Neurophysiol.*, **94**, 1904–1911.
- Lindén, H., Tetzlaff, T., Potjans, T.C., Pettersen, K.H., Grün, S., Diesmann, M. & Einevoll, G.T. (2011) Modeling the spatial reach of the LFP. *Neuron*, **72**, 859–872.
- Liu, R.C. & Galindo-Leon, E.E. (2010) Predicting stimulus-locked single unit spiking from cortical local field potentials. *J. Comput. Neurosci.*, **29**, 581–597.
- Liu, J. & Newsome, W.T. (2006) Local field potential in cortical area MT: stimulus tuning and behavioral correlations. *J. Neurosci.*, **26**, 7779–7790.
- Logothetis, N.K. (2003) The underpinnings of the BOLD functional magnetic resonance imaging signal. *J. Neurosci.*, **23**, 3963–3971.
- Lorente de No, R. (1947) Analysis of the distribution of the action currents of nerve in volume conductors. *Stud. Rockefeller Inst. Med. Res. Repr.*, **132**, 384–477.
- Luo, F., Wang, Q., Kashani, A. & Yan, J. (2008) Corticofugal modulation of initial sound processing in the brain. *J. Neurosci.*, **28**, 11615–11621.
- Luo, F., Wang, Q., Farid, N., Liu, X. & Yan, J. (2009) Three-dimensional tonotopic organization of the C57 mouse cochlear nucleus. *Hearing Res.*, **257**, 75–82.
- Machens, C.K., Wehr, M.S. & Zador, A.M. (2004) Linearity of cortical receptive fields measured with natural sounds. *J. Neurosci.*, **24**, 1089–1100.
- Martin, A.R. (1976) The effect of membrane capacitance on non-linear summation of synaptic potentials. *J. Theor. Biol.*, **59**, 179–187.
- Metherate, R., Lazar, R. & Simranjit, K. (2004) Intracortical pathways determine breadth of subthreshold frequency receptive fields in primary auditory cortex. *J. Neurophysiol.*, **91**, 2551–2567.
- Metherate, R., Kaur, S., Kawai, H., Lazar, R., Liang, K. & Rose, H.J. (2005) Spectral integration in auditory cortex: mechanisms and modulation. *Hearing Res.*, **206**, 146–158.
- Miller, L.M., Escabi, M.A., Read, H.L. & Schreiner, C.E. (2001) Functional convergence of response properties in the auditory thalamocortical system. *Neuron*, **32**, 151–160.
- Miller, L.M., Escabi, M.A., Read, H.L. & Schreiner, C.E. (2002) Spectrotemporal receptive fields in the lemniscal auditory thalamus and cortex. *J. Neurophysiol.*, **87**, 516–527.
- Mitzdorf, U. (1985) Current source-density method and application in cat cerebral cortex: investigation of evoked potentials and EEG phenomena. *Physiol. Rev.*, **65**, 37–100.
- Moeller, C.K., Kurt, S., Happel, M.F. & Schulze, H. (2010) Long-range effects of GABAergic inhibition in gerbil primary auditory cortex. *Eur. J. Neurosci.*, **31**, 49–59.
- Mormann, F., Fell, J., Axmacher, N., Weber, B., Lehnertz, K., Elger, C.E. & Fernández, G. (2005) Phase/amplitude reset and theta-gamma interaction in the human medial temporal lobe during a continuous word recognition memory task. *Hippocampus*, **15**, 890–900.
- Muller, C.M. & Scheich, H. (1988) Contribution of GABAergic inhibition to the response characteristics of auditory units in the avian forebrain. *J. Neurophysiol.*, **59**, 1673–1689.
- Noreña, A.J. & Eggermont, J.J. (2002) Comparison between local field potentials and unit cluster activity in primary auditory cortex and anterior auditory field in the cat. *Hearing Res.*, **166**, 202–213.
- Noreña, A.J., Gourévitch, B., Pienkowski, M., Shaw, G. & Eggermont, J.J. (2008) Increasing spectrotemporal sound density reveals an octave-based organization in cat primary auditory cortex. *J. Neurosci.*, **28**, 8885–8896.
- Nunez, P.L. (2006) *Electric Fields of the Brain: The Neurophysics of EEG*. Oxford University Press, Oxford.
- Rasch, M., Logothetis, N.K. & Kreiman, G. (2009) From neurons to circuits: linear estimation of local field potentials. *J. Neurosci.*, **29**, 13785–13796.
- Schroeder, C.E., Mehta, A.D. & Givre, S.J. (1998) A spatiotemporal profile of visual system activation revealed by current source density analysis in the awake macaque. *Cereb. Cortex*, **8**, 75–92.
- Suga, N., Zhang, Y. & Yan, J. (1997) Sharpening of frequency tuning by inhibition in the thalamic auditory nucleus of the mustached bat. *J. Neurophysiol.*, **77**, 2808–2814.
- Wang, J., Caspary, D. & Salvi, R.J. (2000) GABA-A antagonist causes dramatic expansion of tuning in primary auditory cortex. *NeuroReport*, **11**, 1137–1140.
- Wang, J., McFadden, S.L., Caspary, D. & Salvi, R. (2002) Gamma-aminobutyric acid circuits shape response properties of auditory cortex neurons. *Brain Res.*, **944**, 219–231.
- Wehr, M. & Zador, A.M. (2005) Synaptic mechanisms of forward suppression in rat auditory cortex. *Neuron*, **47**, 437–445.
- Xing, D., Yeh, C.I. & Shapley, R.M. (2009) Spatial spread of the local field potential and its laminar variation in visual cortex. *J. Neurosci.*, **29**, 11540–11549.
- Yan, J. & Ehret, G. (2002) Corticofugal modulation of midbrain sound processing in the house mouse. *Eur. J. Neurosci.*, **16**, 119–128.
- Yan, J. & Zhang, Y. (2005) Sound-guided shaping of the receptive field in the mouse auditory cortex by basal forebrain activation. *Eur. J. Neurosci.*, **21**, 563–576.
- Zhang, Y., Dyck, R.H., Hamilton, S.E., Nathanson, N.M. & Yan, J. (2005) Disrupted tonotopy of the auditory cortex in mice lacking M1 muscarinic acetylcholine receptor. *Hearing Res.*, **201**, 145–155.